Acta. Chim. Asiana., 2026, 9(2), 920-930
e-ISSN/p-ISSN 2550-0503/2550-049x
Available online at: www.aca.unram.ac.id

RESEARCH PAPER

A Simple Low-Cost Paper-Based Analytical Device For Detecting Water Hardness

Edy Agustian Yazid[a]* and Abdul Wafi [b]

[a]Department of Medical Laboratory Technology, Delima Husada Gresik Health Analyst Academy, Gresik 61111, Indonesia

[b]Research Center for Food Technology and Processing, National Research and Innovation Agency (BRIN), Playen, Gunungkidul, Yogyakarta 55861, Indonesia

E-mail: estien_y@yahoo.com

DOI: https://doi.org/10.29303/aca.v9i2.310

Article info:

Received: 18/06/2026

Revised: 02/10/2026

Accepted: 05/11/2026

Available online: 11/11/2026

Abstract: High water hardness triggers piping system damage and adverse health effects, necessitating regular monitoring. This study aims to develop a simple, low-cost, and user-friendly paper-based analytical device (PAD) for on-site water hardness detection. The device was fabricated by immobilizing Eriochrome Black T (EBT) indicator and a pH 10 buffer onto a paper matrix based on complexometric reaction principles. Analytical performance evaluation demonstrated that the PAD could detect water hardness within the 50–350 ppm concentration range with strong linearity (R^2 = 0.9991). The sensor exhibited LOD and LOQ values of 47.16 ppm and 157.19 ppm, respectively; precision (RSD) between 0.32% and 4.30%; and recovery rates ranging from 108.02% to 114.04%, with a rapid response time of 5 seconds. Quantitative data analysis was performed colorimetrically using smartphone-based digital imaging and RGB analysis. Testing on real water samples yielded good accuracy and clear visual color contrast corresponding to increasing concentrations, confirming the sensor platform's high sensitivity. In conclusion, this PAD offers a practical, rapid, and portable analytical alternative that requires neither complex laboratory equipment nor specialized operational expertise, making it highly suitable for on-site water quality monitoring.

Keywords: Paper-based analytical device; water hardness; colorimetric detection; Water quality monitoring

INTRODUCTION

Water is a fundamental necessity for human survival and requires strict health standards to prevent adverse public health and socioeconomic consequences. Unsafe water has a wide impact on the risk of various chronic diseases and infections, as well as cardiovascular and maternal-neonatal disorders [1-3]. Water plays a fundamental macroeconomic and social role, from basic domestic uses to driving productive economic sectors. At a fundamental level, water is essential for direct human consumption, sanitation, and food preparation, and serves as a vital resource for industrial, agricultural, and fisheries operations (4-6]. Given its vital role, water resource management and conservation must be implemented sustainably [7].

Currently, the availability of water resources is facing the challenge of declining quality and quantity, resulting in an inability to meet surging demand, particularly for the domestic sector [8]. This decline in water quality has the potential to trigger ecological disruption and environmental damage [9]. Water quality degradation, both in aquifers and river bodies, has impacted the ability of water resources to provide safe and healthy clean water standards for the community. Clean water is an integrated quality standard encompassing three main parameters, including physical, chemical, and microbiological [10-12].

Water hardness is a crucial chemical parameter for assessing water quality [13]. Water hardness is a total concentration of calcium ions (Ca^{2+}) and magnesium ions (Mg^{2+}), which are usually expressed as calcium carbonate equivalents ($CaCO_3$) in milligrams per liter (mg/L) or part per million (ppm) [14]. Dissolved calcium and magnesium are two types of divalent cations found in significant amounts in most water sources. In natural waters, calcium and magnesium are often bound to bicarbonate, sulfate, or chloride. Besides, calcium and magnesium, other dissolved divalent metals, such as iron, copper, zinc, and lead, also contribute to total hardness. However, naturally occurring concentrations of these divalent metals in

water are so small (trace) that they can be ignored [15].

Water hardness, primarily driven by elevated calcium (Ca^{2+}) and magnesium (Mg^{2+}) ions, poses significant challenges in both domestic and industrial settings. In households, it diminishes soap efficacy by binding with fatty acids to form insoluble scum and causes scaling on appliances. Industrially, uncontrolled hardness leads to severe scaling, which drastically reduces the thermal efficiency of boilers and turbines, and creates explosion hazards due to restricted heat transfer [16-18]. Furthermore, prolonged consumption of hard water is clinically linked to an increased risk of nephrolithiasis and cardiovascular diseases [18-20]. Water hardness classification standards are based on the potential for scale formation. Water with a hardness of 300–350 ppm is categorized as very hard, and water above 350 ppm is categorized as aggressively hard, which risks damaging pipes. Based on regulations, the Indonesian Ministry of Health sets the maximum limit for water hardness for sanitation, hygiene, and drinking water purposes at 500 ppm mg/L [21-22].

Quantitative analysis of water hardness has been performed using several methods, including titrimetry (complexometry) [23-24], automated titration systems [25], spectrophotometry [24], and atomic absorption spectroscopy (AAS) [26]. Advanced quantitative technologies, including laser-induced breakdown spectroscopy (LIBS) [27], inductively coupled plasma mass spectrometry (ICP-MS) [28], image-based titration systems [29], and lateral flow-based paper-based distance sensors [30], offer high accuracy, low detection limits, and digital data recording capabilities. However, these instrumental approaches are limited by their relatively high cost, high reliance on specialized laboratories, and complex operating procedures. Qualitative or semi-quantitative analysis, on the other hand, is generally performed through soap suds tests, heating, and chemical precipitation [31]. Although simple and economical, these conventional methods suffer from low precision, limited detection ranges, and are heavily influenced by subjective visual interpretation.

This technical gap drives the urgent need for a portable platform that can combine the ease of qualitative testing with reliable semi-quantitative accuracy in the field. One method currently being widely developed is a paper-based analytical device (PAD) platform with colorimetric detection. This platform offers the advantages of cost-effectiveness, simplicity, and ease of interpretation through visual color changes as an indicator of the target analyte's presence [32-33]. In addition to colorimetric techniques, other approaches such as chemiluminescence (CL) [34], electro-chemiluminescence (ECL) [35], fluorescence [36], and electrochemical [37] detection have been used to monitor analytes. However, these techniques have operational limitations for field testing. CL and ECL techniques suffer from rapid signal decay and require complex fluids or fragile electrode modifications. Fluorescence relies on external excitation and is susceptible to photobleaching, while electrochemical sensors are susceptible to baseline shifts and environmental noise. These limitations highlight the advantages of instrument-free visual colorimetric paper devices for rapid water hardness screening.

Although various PAD have been successfully implemented for environmental monitoring, analytical tools specifically designed for water hardness analysis remain limited. Previously reported lateral-flow distance-based paper sensors tend to be complex and require analysis times spanning minutes, as they rely on regulating fluid viscosity (using Na-alginate). The PAD developed in this study offers distinct innovations in terms of fabrication efficiency and operational simplicity through the integration of a simple immobilization technique without complicated chemical modifications between the Eriochrome Black T (EBT) indicator and pH 10 buffer on a paper matrix. This approach effectively maintains reagent stability, minimizes chemical volume, and produces sharp, contrasting, and homogeneous color transitions upon interaction with Ca^{2+} and Mg^{2+} ions within seconds. These characteristics not only enable semi-quantitative estimation directly on-site by users without specialized laboratory training but also support precise digital quantification through smartphone-based imaging. The color intensity analysis of the imaging results is then evaluated using the RGB (Red, Green, Blue) color model system through ImageJ software. Furthermore, the platform's analytical performance has been comprehensively validated based on its linear dynamic range, limit of detection (LOD), limit of quantification (LOQ), precision, and accuracy. Thus, this pioneering platform provides a robust, low-cost, and practical alternative for rapid on-site water quality monitoring, particularly suitable for resource-constrained environments.

MATERIALS AND METHODS

Chemicals and instrumentation

All of the reagents and chemicals used in this study are analytical grades obtained from Sigma-Aldrich (Merck). The materials used are calcium carbonate ($CaCO_3$), hydrochloric acid (HCl), Eriochrome Black T (EBT), Ammonium chloride (NH_4Cl), ammonium

hydroxide (NH_4OH), and demineralized water. Water samples were taken directly from Gresik City. All solutions are prepared in demineralized water and stored in dark bottles at room temperature.

The absorption spectra were measured using a UV-1600PC (VWR) spectrophotometer using a 1.0 cm quartz cuvette. Other equipment supporting the analysis included an analytical balance, pH meter (Merck Hanna), oven, desiccator, microburette, a set of laboratory glassware, Whatman Grade 1 filter paper and waterproof synthetic paper. All glassware was cleaned with HCl: HNO_3 (3:1) and rinsed with demineralized water before use. Images were captured using a smartphone (Vivo V50 Lite 5G; 50 MP camera resolution, Sony IMX882 sensor). The obtained images were analyzed using the ImageJ program (RGB color mode).

PAD Fabrication Preparation

The reagent absorbent substrate was prepared using Whatman filter paper that had been heated in an oven at 110°C for 1 minutes. Substrate immobilization was performed by immersing the paper in a pH 10 buffer solution of optimal concentration for 30 minutes in a closed container. During the immersion process, the paper was periodically turned over to ensure even reagent absorption. The same procedure was applied to the immobilization stage of the EBT indicator of optimal concentration. The paper containing both reagents was then dried in a desiccator for 48 hours. The dried substrate was glued to synthetic matte paper waterproof and cut to size. The device, as a colorimetric sensor, was designed to resemble universal pH indicator paper, thereby increasing its practicality and portability. The device was stored in a tightly closed container at room temperature and was ready to be used for hardness analysis in water samples.

PAD Characterization

The PAD was used to test water samples containing a certain level of hardness. The color change of the paper from blue to red was captured using a smartphone on a white background in a well-lit area, away from direct sunlight. The resulting image was transferred to a computer, and each color change, including the blank, was extracted using ImageJ/Fiji software. In this program, the color formed in each cell was analyzed based on the RGB (red, green, blue) system. The effective intensity of the color value was calculated based on equations (1), (2), and (3) as follows [38].

$$A_r = -Log\left(\frac{R_S}{R_b}\right) \qquad (1)$$

$$A_g = -Log\left(\frac{G_S}{G_b}\right) \qquad (2)$$

$$A_b = -Log\left(\frac{B_S}{B_b}\right) \qquad (3)$$

Where *Ar*, *Ag*, and *Ab* are the effective intensities for red, green, and blue. *Rs*, *Gs*, *Bs*, and *Rb*, *Gb*, *Bb* are the red, green, and blue values of the sample and blank, respectively. The platform was further validated based on its dynamic linear range, limit of detection (LOD), limit of quantification (LOQ), precision, and accuracy.

PAD Application

The PAD performance was evaluated based on colorimetric changes caused by the presence of Ca^{2+} and Mg^{2+} metal ions. The detection mechanism of the PAD is based on the principle of standard complexometric titration, where the EBT indicator binds with Ca^{2+} and Mg^{2+} ions simultaneously at pH 10. The complexation of these divalent cations induces a distinct color transition from blue to wine red. The intensity of the color response generated by the PAD directly represents the total water hardness expressed as $CaCO_3$ equivalent.

.The testing procedure involves dipping the tip of the device into the water until the entire detection area is submerged for a few moments, then removing it. If the sample is too acidic, it must first be neutralized or adjusted to a pH range of 6.5–8.5. This step ensures the maintenance of the detection zone's buffer capacity, thereby preventing interference with the stability of the metal-EBT complex and the indicator's specific color transition. The color change of the paper in the detection area from blue to red indicates a certain level of hardness in the water sample. The resulting color intensity is then compared with the color in the standard solution. The red image provides quantitative information extracted using the ImageJ/Fiji software program.

RESULTS AND DISCUSSION

Optimization of Experimental Conditions

Optimization of experimental conditions affecting the absorption of Ca^{2+} metal ions using immobilized reagents has been investigated. This aims to determine the appropriate reagent concentration to produce optimal absorption during red color formation, thereby increasing analytical sensitivity. The optimum reagent concentration is determined based on the level of the most significant color change [39]. In paper-based colorimetric sensors, clear, intense, and uniform color changes indicate that the reagent particles have been effectively and evenly immobilized on the paper fiber structure [40].

Acta. Chim. Asiana., 2026, 9(2), 920-930
e-ISSN/p-ISSN 2550-0503/2550-049x
Available online at: www.aca.unram.ac.id

RESEARCH PAPER

Eriochrome Black T (EBT) indicators at pH 10 or close to neutral, especially as azo-naphthol deprotonation shows a blue color. Hard water contains a considerable concentration of divalent metal ions, especially Ca^{2+} and Mg^{2+}. These metal ions form a red chelate complex with EBT at pH 10. The formation of the EBT-metal complex changes the conjugation and distribution of the metal-ligand charge, shifting the spectrum of its absorption. The EBT-Ca^{2+}/Mg^{2+} complex absorbs light differently and appears burgundy (pink-red). The reaction of the formation of complex compounds between EBT and Ca^{2+}/Mg^{2+} ions is shown in equations (4) and (5).

$$\text{EBT (Dark purple)} \xrightarrow{\text{(pH = 10)}} \text{EBT (Blue)} \quad (4)$$

$$\text{EBT (Blue)} + Ca^{2+}/Mg^{2+} \xrightarrow{\text{(pH = 10)}} \text{EBT–}Ca^{2+}/Mg^{2+}\text{ (Red)} \quad (5)$$

The intensity of the red color formed is proportional to the number of Ca^{2+} and Mg^{2+} ions bound by EBT.

Effects of pH and EBT

The effect of pH 10 buffer solution and EBT indicator was evaluated to obtain the optimal EBT–Ca^{2+} complex formation. Spectrophotometric analysis in the range of 400–800 nm showed the maximum absorbance of the EBT–Ca^{2+} complex at λ= 540 nm. The optimum condition was achieved by adding 2.0 mL of pH 10 buffer (Figure 1). Under this condition, the EBT molecule is completely deprotonated, thus binding maximally with calcium ions. The addition of EBT indicator gave the best absorbance at the addition of 0.433 µmol (Figure 2). This optimization prevented the effects of self-absorption and weak signals, thereby increasing the sensitivity and accuracy of the proposed analytical device.

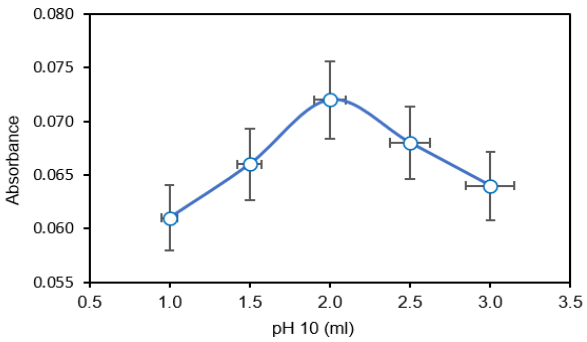


Figure 1. Effect of pH 10 buffer solution on EBT-Ca^{2+} complex formation

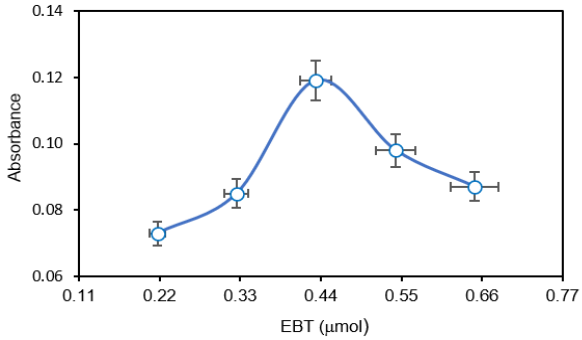


Figure 2. Effect of EBT indikator on EBT-Ca^{2+} complex formation

PAD Fabrication

The PAD was fabricated using a mixture containing a buffer solution and an EBT indicator. Whatman Grade 1 chromatography paper was selected as the absorbent substrate due to its superior wicking properties. This specific paper substrate features a pore size of 11 µm and a thickness of 180 µm, which facilitates medium flow rates and uniform capillary action for fluid migration. Its pure cellulose fiber composition ensures excellent reagent compatibility, high hydrophilicity, and chemical stability across a wide pH range without interfering with the reagent molecules [41–43]. The fabrication of a single-detection-zone-based dipstick assay represents one of the most straightforward approaches. This process involves sequentially saturating the paper with the buffer and reagents through immersion. Once dried, the functionalized paper is attached to a non-reactive, waterproof synthetic paper backing, which serves as a handle [44].

The process of immobilizing reagents on paper is greatly influenced by soaking time, temperature, and drying time. Each layer of reagent must be completely dry before immobilizing the next layer. This ensures that all reagents required for the chemical reaction on the paper can be optimally distributed and absorbed. Drying at extreme temperatures or exposure to direct sunlight in open spaces should be avoided, as this can accelerate the evaporation of the buffer solution and damage the stability of the indicator.

Furthermore, fluctuations or decreases in the concentration of the buffer solution will directly impact the stability and accuracy of the color changes of indicators such as Eriochrome Black T. Figure 3 presents a schematic illustration of the proposed device fabrication procedure.

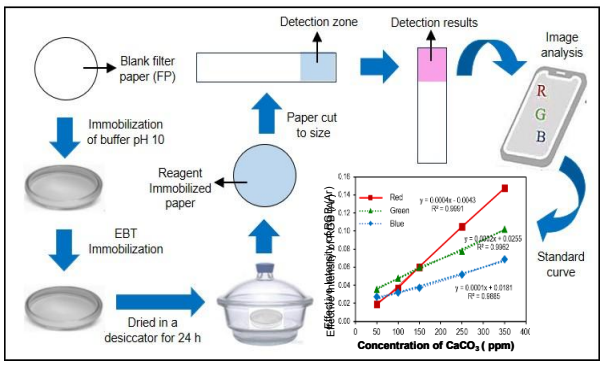


Figure 3. Schematic illustration of the PAD fabrication procedure for detecting water hardness

Analytical Performance and Calibration Curves

The proposed PAD demonstrated excellent analytical performance. A recovery percentage close to 100% indicates high accuracy of the developed method. The calibration curve, established between $CaCO_3$ concentration and the effective red color intensity, exhibited strong linearity (R^2 = 0,9991) within the concentration range of 50–350 ppm. Furthermore, the sharp increase in red color intensity reflects the high sensitivity of the method. A low relative standard deviation (RSD) confirms excellent precision and reproducibility (Table 1). The calibration curve of the proposed method is illustrated in Figure 4.

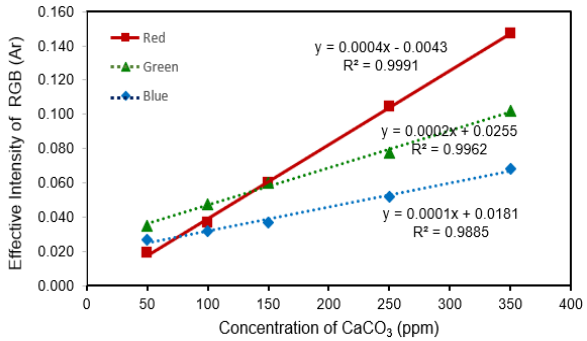


Figure 4. Calibration curve of $CaCO_3$ standard solution

Based on the calibration curve, three equations were obtained for red, green, and blue. The best regression equation was obtained for the red color regression equation, namely, y = 0.0004x - 0.0043, with a correlation coefficient (r) of 0.999 (Figure 4). The *r*-value is close to 1.0 ($r \geq 0.999$ or $R^2 \geq 0.9991$), indicating a very strong linear relationship between analyte concentration and absorption [45]. This means that the change in analyte concentration is directly proportional to the change or response of the sensor on the paper. The relationship between concentration and hardness absorption shows that the higher the hardness concentration, the higher the formation of red color on the paper.

Table 1. Characteristics of the proposed method for the detection of water hardness

Parameters	Value
Maximum wavelength (nm)	540
Color	Red
Beer Law concentration range (ppm)	50 - 350
Detection limit (LOD) (ppm)	47.16
Quantification limit (LOQ) (ppm)	157.19
Regression parameters	
Slope (Sb)	0.0004
Intercept (Sa)	-0.0043
Correlation coefficient (*r*)	0.999
Recovery (%)	108.02 - 114.04
Standard Relative Deviation (%RSD)	0.32 - 4.30

Accuracy and Precision

Accuracy and precision were verified using five standard solutions with different concentrations across the linear range. Each parameter was determined through five replicate analyses using different devices. Relative error (%Erel) was evaluated to assess the bias between theoretical and measured concentrations. The results showed an average positive bias of 8.36%, attributed to the coffee-ring effect on the paper matrix and fluctuations in ambient lighting. Nevertheless, the method demonstrated good precision, with relative standard deviation (RSD) values ranging from 0.32% to 4.30% (RSD < 5%) and recovery percentages between 108.02% and 114.04%. These recovery values fall within the acceptable limits for on-site analysis methods (98–115%) at the parts-per-million (ppm) concentration level [46]. This indicates that RGB color analysis is highly suitable for semi-quantitative purposes, whereas precise and accurate quantitative analysis can be achieved using the calibration curve equation. Detailed results regarding the accuracy and precision of the proposed method are summarized in Table 2.

Table 2. Accuracy and precision of the proposed method*

$CaCO_3$ given (ppm)	$CaCO_3$ obtained (ppm)	SD	RSD (%)	Recovery (%)	E_{rel} (%)
50	57.02	2.45	4.30	114.04	-14.04
100	103.92	2.25	2.17	103.92	-3.92
150	161.29	2.86	1.77	107.52	-7.52
250	270.80	3.26	1.21	108.32	-8.32
350	378.08	1.20	0.32	108.02	-8.02

*) *Five replicas*

Sensitivity

The method's sensitivity was evaluated to assess the PAD's ability to detect water hardness, as indicated by the Limit of Detection (LOD) and Limit of Quantification (LOQ). The LOD is the lowest detectable analyte concentration, while the LOQ is the lowest concentration that can be quantitatively measured with acceptable precision and accuracy [47]. The proposed PAD responded within 5 seconds, with an LOD of 47.16 ppm and an LOQ of 157.19 ppm. Based on these limits, the PAD's analytical performance was classified into three categories: qualitative detection at concentrations below the LOD (<47.16 ppm), semi-quantitative estimation in the range of 47.16–157.19 ppm, and full quantification with high precision in the range of 157.19–350 ppm, which falls within the device's optimal dynamic operating range.

PAD Functionalization

The functionalization of PADs for analytical applications can be significantly enhanced by increasing the sensitivity of colorimetric detection [48]. Various strategies can be employed by using highly effective reagents, enhancing the efficiency of chromogenic reagent immobilization on paper, optimizing reaction conditions, selecting suitable paper substrates, and developing visualization methods [49-50]. In this study, the optimization of Eriochrome Black T (EBT) concentration and buffer solution at pH 10 was investigated to obtain the maximum absorption response during the reaction. The appearance of a red color indicates that the EBT reagent and buffer solution have been optimally immobilized on the paper. This facilitates the formation of a more intense red EBT–Ca^{2+} complex on the device. The formation of the color complex is evenly distributed, resulting in stronger visual sensitivity, even at low Ca^{2+} ion concentrations.

Response Time and Operating Time

Response time and operating time were evaluated to determine device stability. Response time indicates the ability of the paper-based sensor to interact with the analyte upon initial contact with the test solution, which typically ranges from a few minutes to 30 minutes. The faster the response time, the better the device performance [51-52]. Visual observation of the device showed rapid red color formation, with the detection process taking place within 5 seconds. Color development was monitored for 15 minutes, and color intensity was analyzed using the RGB color system. The analysis results showed that the blue color intensity reached a steady state at 10 minutes. Therefore, 10 min was selected as the actual measurement time for both quantitative and semi-quantitative analyses to ensure data accuracy and reproducibility.

The operational performance of the PAD was evaluated to determine its effectiveness in detecting Ca^{2+} ions, resulting in a stable and consistent response. Sensor stability refers to the sensor's ability to maintain consistent performance over time, particularly under fluctuating environmental conditions [53]. Degradation in sensor performance is typically detected when the analytical response decreases by more than 15% from the initial response [54-55]. The color intensity was measured in triplicate for each testing interval daily during the first week, and weekly thereafter until the maximum red intensity decreased by 15%. The evaluation results indicated that the PAD was stable and functioned optimally for up to eight weeks of storage. In this test, the device was stored in a tightly closed plastic container at room temperature (25°C-30°C).

RGB Profile

The RGB profile evaluation was performed based on colorimetric images obtained from the reaction between the EBT indicator and Ca^{2+} metal ions in a standard $CaCO_3$ solution. The images were converted into color intensity data to generate RGB

curve profiles, representing the relationship between pixel distance and color intensity as a function of brightness (Figure 5). The curves show that the red channel produces a higher intensity level compared to the other two channels (green and blue). All three color channels exhibit parallel fluctuations along the pixel spacing. This indicates that minor variations in intensity are influenced by the substrate texture or lighting factors, rather than by inconsistencies in the chemical reaction. This consistent pattern confirms excellent color homogeneity in the paper spots, thus ensuring the reliability and reproducibility of the colorimetric readings. This indicates that higher water hardness levels lead to an increase in the intensity of the red color formed on the paper. Based on the calibration curve, the red color intensity reaches saturation at a concentration of 350 ppm (Figure 6b).

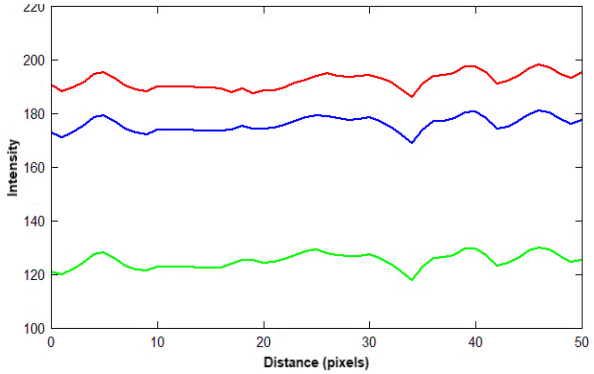


Figure 5. RGB profile of the EBT-Ca complex

PAD Application

Before its application to water samples, PAD was evaluated using a standard $CaCO_3$ solution as a positive control and demineralized water as a negative control (blank). Visual inspection of the color chart (Figure 6b) revealed a significant color contrast, shifting from blue (cyan) at a concentration of 0 ppm (blank) to purplish red with increasing concentrations up to 350 ppm. The distinct visual contrast observed between 0 ppm and 50 ppm indicates the high sensitivity of the sensor system at low concentrations, which is triggered by the initial phase of metal-ligand complex formation. Within the concentration range of 100–350 ppm, a gradual color shift toward red (saturated magenta) occurs. Although the visual differentiation between concentration levels in this higher range becomes narrower due to the natural saturation limits of the chromophore groups and the optical resolution of the human eye, each gradation remains macroscopically distinguishable. This color evolution represents a shift in chemical equilibrium resulting from the formation of the metal-indicator complex as more Ca^{2+} ions bind to the chromogenic ligand.

The linearity and statistical significance of the method were evaluated using linear regression analysis across a $CaCO_3$ concentration range of 50–350 ppm (n = 5) (Figure 6). The resulting calibration curve demonstrated a strong positive correlation, with a correlation coefficient (r) of 0.999 and a coefficient of determination (R^2) of 0.9991. This indicates that changes in the $CaCO_3$ concentration can linearly explain 99.91% of the variation in the effective RGB intensity. To statistically test the model's significance, analysis of variance (ANOVA) was performed using the F-test at a 95% confidence level (α= 0.05; df = 1,3). The analysis yielded an F-$_{calculated}$ value of 3330.33, which substantially exceeds the F-$_{table}$ value of 10.13. The validity of this model is further supported by a p-value of <0.0001, falling well below the critical threshold of 0.05. These findings empirically demonstrate that the developed regression model is highly significant and exhibits robust linearity for quantitative analysis.

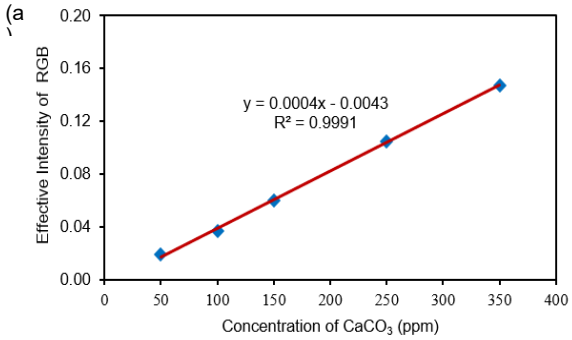


Figure 6. Formation profile of red color on the test strip. (a), Linear regression of calibration curves and (b), Formation of red color at various concentrations of standard solutions

The PAD was subsequently applied to field water samples to detect Ca^{2+} and Mg^{2+} ions, which represent the total water hardness. The appearance of a red color in the detection zone was visually observed and compared against standard solutions (Figure 6b). Test results were read semi-quantitatively using a graded scale ranging from positive (+1) to (+4), which could be converted into mg/L units. Potential interference from other divalent metal ions such as Fe^{2+}, Cu^{2+}, Zn^{2+}, and Pb^{2+} was considered negligible, as their concentrations in natural water samples were at trace levels and thus did not affect color complex formation. Of the five water samples tested, four yielded positive results, indicated by a distinct red color change in the

detection zone. Conversely, one sample showed a negative result with no significant color change, indicating that the concentration of the target ions in that sample was below the detection limit of the developed PAD device.

Table 3 presents the results of semi-quantitative and quantitative analyses of the total hardness of the five water samples tested. Semi-quantitative testing on mountain water samples yielded negative results with estimated total hardness in the range of 0–50 ppm. Meanwhile, water samples from the Regional Drinking Water Company (RDWC) showed a positive result of one (+1) in the range of 50–100 ppm. River water samples yielded a positive result of two (+2) in the range of 100–150 ppm, while borehole water and seawater both yielded a positive three (+3) in the range of 150–250 ppm. The results of quantitative analysis through the calibration curve equation showed the total hardness levels in order: mountain water (39.78 ppm), water from RDWC (70.40 ppm), river water (116.22 ppm), borehole water (171.87 ppm), and seawater (197.43 ppm). The highest hardness concentration was obtained in seawater samples, which was influenced by the high content of dissolved salts such as calcium, magnesium, chloride, and sulfate, which were calculated as equivalent to calcium carbonate ($CaCO_3$).

Table 3. Semi-quantitative and quantitative total hardness rate.

Water sample	Visual observation	Total hardness (ppm)	
		Semi-kuantitative	Quantitative
Mountain	egatives	< 50	39.78
RDWC		50-100	70.40
Borewell	+	150-250	171.87
River		100-150	116.22
Sea	+	150-250	197.43

CONCLUSION

This study successfully developed a simple and low-cost paper-based analytical device (PAD) aiming to provide a practical, rapid, and portable water quality monitoring method for detecting water hardness. Based on the experimental evaluation, the proposed PAD was capable of operating within a concentration range of 50–350 ppm with a 5-second response time, demonstrating strong linearity (R^2 = 0.9991), alongside acceptable precision (RSD of 0.32%–4.30%) and accuracy for semi-quantitative on-site analysis. The significance of this research lies in its ability to offer an affordable and user-friendly testing alternative without relying on complex laboratory equipment or specialized operational expertise. Looking ahead, this platform holds great potential to be integrated with mobile applications for more automated colorimetric digitization, and it can be further developed for the on-site detection of other environmental contaminants.

ACKNOWLEDGEMENTS

The authors would like to thank the Delima Husada Gresik Health Analyst Academy for providing facilities for this research.

REFERENCES

[1] Paudel, S., Kumar, P., Dasgupta, R., Johnson, B. A., Avtar, R., Shaw, R., .& Kanbara, S. (2021). Nexus between water security framework and public health: A comprehensive scientific review. *Water*, *13*(10).1365. doi:10.3390/w13101365.

[2] Russ, J., Zaveri, E., Desbureaux, S., Damania, R., & Rodella, A. S. (2022). The impact of water quality on GDP growth: Evidence from around the world. *Water Security*, *17*, 100130. doi:10.1016/j.wasec.2022.100130.

[3] Li, S., Wei, Y., Zhou, J., Li, Y., Qiao, L., You, D., ... & Ma, X. (2026). Unsafe drinking water and human health: A global umbrella review of disease outcomes, intervention effectiveness, and policy implications. *Cell Reports Medicine*. 7, 102588, doi:10.1016/j.xcrm.2026.102588.

[4] Crouch, M. L., Jacobs, H. E., & Speight, V. L. (2021). Defining domestic water consumption based on personal water use activities. *AQUA—Water Infrastructure, Ecosystems and Society*, *70*(7), 1002-1011. doi:10.2166/aqua.2021.056.

[5] Ahmad, R. A. R., Ab Aziz, N. H., Zainon, S., & Nur, A. (2022). Evaluating The Usage of Domestic Water for Good Health and Well Being, 2(2), 511-514. doi:10.6007/IJARAFMS/v12-i2/14122.

[6] Ibrahim, L. A., Abu-Hashim, M., Shaghaleh, H., Elsadek, E., Hamad, A. A. A., & Alhaj Hamoud, Y. (2023). A comprehensive review of the multiple uses of water in aquaculture-integrated agriculture based on international and national experiences. *Water*, *15*(2), 367. doi:10.3390/w15020367.

[7] Ciampittiello, M., Marchetto, A., & Boggero, A. (2024). Water resources management under climate change: a review. *Sustainability*, *16*(9), 3590. doi:10.3390/su16093590.

[8] Lund Schlamovitz, J., & Becker, P. (2021). Differentiated vulnerabilities and capacities for adaptation to water shortage in Gaborone, Botswana. *Int. J. Water Resour*, *37*(2), 278-299. doi:10.1080/07900627.2020.1756752.

[9] Schwarzenbach, R. P., Egli, T., Hofstetter, T. B., Von Gunten, U., & Wehrli, B. (2010). Global water pollution and human health. *Annual review of environment and resources*, *35*, 109-136. doi:10.1146/annurev-environ-100809-125342.

[10] Misman, N. A., Sharif, M. F., Chowdhury, A. J. K., & Azizan, N. H. (2023). Water pollution and the assessment of water quality parameters: a review. *Desalination and Water Treatment*, *294*, 79-88. doi:10.5004/dwt.2023.29433.

[11] Katili, I., Baderan, D. W. K., & Kumaji, S. S. (2023). Analysis of drinking water quality based on biological, physical and chemical parameters in Lekobalo Village, Gorontalo City, Indonesia. *International Journal of Bonorowo Wetlands*, *13*(1), 22-29. doi:10.13057/bonorowo/w130104.

[12] Purba, A. S., Pratiwi, A. N., Sunari, T., Salim, A., & Candraningrum, R. G. S. (2026). Evaluation of Drinking Water Quality Based on Quality Standards as a Guarantee of Food Safety in Serang Regency. *Journal of Food and Agricultural Product*, *6*(1), 195-208. doi:10.32585/jfap.v6i1.8034.

[13] Nasim, I., Nawaz, R., Farwa, A., Ahmad, S., Irshad, M. A., Al-Hussain, S. A., & Zaki, M. E. (2026). Water quality index and human health risk analysis in urban drinking water sources. *Scientific Reports*, 16, 12831. doi:10.1038/s41598-026-42789-1.

[14] Ingin, Y. P., Mahringer, D., & El-Athman, F. (2024). Hardness properties of calcium and magnesium ions in drinking water. *Applied Food Research*, *4*(2), 100600. doi:10.1016/j.afres.2024.100600.

[15] Sengupta, P. (2013). Potential health impacts of hard water. *International journal of preventive medicine*, *4*(8), 866-875.

[16] Abeliotis, K., Candan, C., Amberg, C., Ferri, A., Osset, M., Owens, J., & Stamminger, R. (2015). Impact of water hardness on consumers' perception of laundry washing result in five European countries. *International Journal of Consumer Studies*, *39*(1), 60-66. doi:10.1111/ijcs.12149.

[17] Kose, A. B., Nikam, N. V., Jaju, S. B., & Khond, V. W. (2024). A review on methods of water softening processes for improving efficiency of bio-mass fired boiler. *Materials Today: Proceedings*, *103*, 383-387. doi:10.1016/j.matpr.2023.09.031.

[18] Dey, S., Veerendra, G. T. N., Manoj, A. V. P., & Padavala, S. S. A. B. (2024). Removal of chlorides and hardness from contaminated water by using various biosorbents: A comprehensive review. *Water-Energy Nexus*, *7*, 39-76. doi:10.1016/j.wen.2024.01.003.

[19] Bykowska-Derda, A., Spychala, M., Czlapka-Matyasik, M., Sojka, M., Bykowski, J., & Ptak, M. (2023). The relationship between mortality from cardiovascular diseases and total drinking water hardness: systematic review with meta-analysis. *Foods*, *12*(17), 3255. doi:10.3390/foods12173255

[20] Zhang, J., Luo, H., Wu, H., Qian, Y., Tang, Z., Wang, J., & He, Z. (2025). The association between domestic water hardness and kidney stone disease: a prospective cohort study from the UK Biobank. *International Journal of Surgery*, *111*(2), 1957-1967. doi:10.1097/JS9.0000000000002198

[21] Kemenkes RI. (2010). *Peraturan Menteri Kesehatan Republik Indonesia Nomor 492/Menkes/Per/IV/2010 tentang Persyaratan Kualitas Air Minum*. Jakarta: Kementerian Kesehatan RI.

[22] Kemenkes RI. (2017). *Peraturan Menteri Kesehatan Nomor 32 Tahun 2017 Tentang Standar Baku Mutu Kesehatan Lingkungan dan Persyaratan Kesehatan*. Jakarta: Kementerian Kesehatan RI.

[23] Amelia, S. R., Prakoso, E. N. J., Ferdiyansah, I., Richo, R. A., & Kuncara, Y. B. (2023). Analisis Kadar Kesadahan Total Pada Air Sumur dan Air PDAM Metode Kompleksometri di Kaliabang Bekasi. *Jurnal Sains Teknologi dalam Pemberdayaan Masyarakat*, *4*(2), 115-120. doi:10.31599/3jwxwk69.

[24] Yazid, E. A., Wafi, A., Zahroh, R., & Azizah, N. (2023). Perbandingan Kadar Magnesium pada Air Minum Dalam Kemasan (AMDK) menggunakan Metode Spektrofotometridan Kompleksometri. *Chimica et Natura Acta*, *11*(3), 115-124. doi:10.24198/cna.v11.n3.48122.

[25] Boppana, N. P., Snow, R., Simone, P. S., Emmert, G. L., & Brown, M. A. (2023). A low-cost

automated titration system for colorimetric endpoint detection. *Analyst*, *148*(9), 2133-2140. doi:10.1039/d2an02086f.

[26] Bisergaeva, R. A., & Sirieva, Y. N. (2020). Determination of calcium and magnesium by atomic absorption spectroscopy and flame photometry. In *Journal of Physics: Conference Series*. 1691(1), 012055. doi:10.1088/1742-6596/1691/1/012055.

[27] Luo, T., Huang, W., Chen, R., Chen, F., Chen, J., Hu, Z., & Nie, J. (2025). Rapid High-Accuracy Quantitative Analysis of Water Hardness by Combination of One-Point Calibration Laser-Induced Breakdown Spectroscopy and Aerosolization. *Chemosensors*, *13*(8), 271. doi:10.3390/chemosensors13080271.

[28] Nadeau, K., Mester, Z., & Yang, L. (2018). The direct and accurate determination of major elements Ca, K, Mg and Na in water by HR-ICPMS. *Scientific Reports*, *8*(1), 17750. doi:10.1038/s41598-018-34028-z.

[29] da Nobrega Gaiao, E., Martins, V. L., da Silva Lyra, W., de Almeida, L. F., da Silva, E. C., & Araújo, M. C. U. (2006). Digital image-based titrations. *Analytica chimica acta*, *570*(2), 283-290. doi:10.1016/j.aca.2006.04.048.

[30] Liu, Y., Dong, L., Wu, W., Ping, J., Chen, J., & Hu, Q. (2024). A portable lateral flow distance-based paper sensor for drinking water hardness test. *Plos one*, *19*(9), e0308424. doi:10.1371/journal.pone.0308424.

[31] Hadi, V., & Novalina, T. (2023). Analisis kesadahan total ($CaCO_3$), kalsium (Ca^{2+}), magnesium (Mg^{2+}) pada air sumur tanah di Jakarta Utara. *Teknosains: Jurnal Sains, Teknologi Dan Informatika*, *10*(1), 1-11. doi:10.37373/tekno.v10i1.192.

[32] Sarvestani, P. S., Majdinasab, M., Golmakani, M. T., Shaghaghian, S., & Eskandari, M. H. (2024). Development of a simple and rapid dipstick paper-based test strip for colorimetric determination of nitrate and nitrite in water and foodstuffs. *Food Chemistry*, *461*, 140856. doi:10.1016/j.foodchem.2024.140856.

[33] Malik, S., Singh, J., Saini, K., Chaudhary, V., Umar, A., Ibrahim, A. A., Akbar, S., & Baskoutas, S. (2024). Paperbased sensors: affordable, versatile, and emerging analyte detection platforms. *Anal. Methods,* 16, 2777–2809. doi:10.1039/D3AY02258G.

[34] Iranifam, M. (2016). Analytical applications of chemiluminescence systems assisted by carbon nanostructures. *TrAC Trends in Analytical Chemistry*, *80*, 387-415. doi:10.1016/j.trac.2015.08.018.

[35] Ma, X., Gao, W., Du, F., Yuan, F., Yu, J., Guan, Y., & Xu, G. (2021). Rational design of electrochemiluminescent devices. *Accounts of chemical research*, *54*(14), 2936-2945. doi:10.1021/acs.accounts.1c00230.

[36] Zacharis, C. K. (2026). Based Analytical Devices Coupled with Fluorescence Detection and Smartphone Imaging: Advances and Applications. *Sensors*, *26*(3), 1012. doi:10.3390/s26031012.

[37] Kulkarni, R. M., Ranjana, M., Ullal, N., & Sunil, D. (2025). A versatile pH-dependent fluorometric, colorimetric, and electrochemical sensor for H2S monitoring in water. *Journal of Fluorescence*, *35*(6), 4861-4871. doi:10.1007/s10895-024-03902-7.

[38] Singh, A. T., Lantigua, D., Meka, A., Taing, S., Pandher, M., & Camci-Unal, G. (2018). Based sensors: emerging themes and applications. *Sensors*, *18* (9), 2838. doi:10.3390/s18092838.

[39] Ji, T., Nam, G., Hwang, S., Park, M., & Shin, J. H. (2025). Fabrication of patterned paper-based sensors for highly efficient formaldehyde detection. *Talanta Open*, 100541. doi:10.1016/j.talo.2025.100541.

[40] Ma, Y., Li, H., Li, Y., & Wei, D. (2024). Preparation of Paper-Based Fluorescent Sensors and Their Application for the Detection of Cu2+ in Water. *Materials*, *17*(16), 3920. doi:10.3390/ma17163920.

[41] Evans, E., Gabriel, E. F. M., Coltro, W. K. T., & Garcia, C. D. (2014). Rational selection of substrates to improve color intensity and uniformity on microfluidic paper-based analytical devices. *Analyst*, *139*(9), 2127-2132. doi:10.1039/c4an00230j

[42] Martinez, A. W., Phillips, S. T., Whitesides, G. M., & Carrilho, E. (2010). Diagnostics for the developing world: microfluidic paper-based analytical devices, 82(1), 3-10. doi:10.1021/ac9013989.

[43] Li, W., Ma, X., Yong, Y. C., Liu, G., & Yang, Z. (2023). Review of paper-based microfluidic analytical devices for in-field testing of pathogens. *Analytica Chimica Acta*, *1278*, 341614. doi:10.1016/j.aca.2023.341614.

[44] Hillscher, L. M., Liebich, V. J., Avrutina, O., Biesalski, M., & Kolmar, H. (2021). Functional paper-based materials for diagnostics. *ChemTexts*, 7, 1–22. doi:10.1007/s40828-021-00139-w.

[45] Yazid, E. A., Zahroh, R., & Hadiyati, A. A. (2022). The Green chili to reduce formaldehyde in tofu by the spectrophotometric method using Schiff reagent. *Natural Science: Journal of Science and*

Technology, *11*(02), 49-57. doi:10.22487/25411969.2022.v11.i02.16144.

[46] Borman, P., & Elder, D. (2017). Q2 (R1) validation of analytical procedures: text and methodology. *ICH quality guidelines: an implementation guide*, 127-166. doi:10.1002/9781118971147.ch5.

[47] Solhtalab, M., Majdinasab, M., Zarei, S., & Majdinasab, E. (2025). Development of a simple and rapid paper-based dipstick test strip for the colorimetric detection of lead and cadmium in water. *Journal of Hazardous Materials Advances*, *19*, 1-15. doi:10.1016/j.hazadv.2025.100867.

[48] Arsawiset, S., & Teepoo, S. (2020). Ready-to-use, functionalized paper test strip used with a smartphone for the simultaneous on-site detection of free chlorine, hydrogen sulfide and formaldehyde in wastewater. *Analytica Chimica Acta*, *1118*, 63-72. doi:10.1016/j.aca.2020.04.041.

[49] Yin, J., Zhang, J., Feng, L., Guan, Y., Gao, W., & Jin, Q. (2022). Free chlorine ultra-sensitive detection in tap water via an enrichment-sensing process by an interdigitated microelectrode sensor. *Electrochimica Acta*, *419*, 1-7. doi:10.1016/j.electacta.2022.140428.

[50] Ampiaw, R. E., Yaqub, M., Woo, C., & Lee, W. (2023). Optimization of disposable paper-based test strips for hypochlorous acid detection. *Membrane Water Treatment*, *14*(4), 181-189. doi:10.12989/mwt.2023.14.4.181.

[51] Tabassum, R., & Kant, R. (2020). Recent trends in surface plasmon resonance based fiber–optic gas sensors utilizing metal oxides and carbon nanomaterials as functional entities. *Sensors and Actuators B: Chemical*, *310*, 1-26. doi:10.1016/j.snb.2020.127813.

[52] Afthoni, M. H., Yunita, S., & Monica, E. (2023). Development of Colloidal Silver-based Mercury Sensors in Whitening Cream. *Pharm. Pharm. Sci. J*, *10*(3). 272-279. doi:10.20473/jfiki.v10i32023.272-279.

[53] Pandey, R., Kumar, P., Sharma, P., & Punia, R. (2023). Challenges and future prospects in bioelectrochemical sensors. *Multifaceted Biosensing Technology*, 4, 99-110. doi:10.1016/B978-0-323-90807-8.00011-7.

[54] Jiang, L., Djurdjanovic, D., Ni, J., & Lee, J. (2006). Sensor degradation detection in linear systems. In *Engineering Asset Management: Proceedings of the 1st World Congress on Engineering Asset Management (WCEAM) 11–14 July 2006* (pp. 1252-1260). London: Springer London. doi:10.1007/978-1-84628-814-2_138.

[55] Kajmakovic, A., Diwold, K., Römer, K., Pestana, J., & Kajtazovic, N. (2022). Degradation detection in a redundant sensor architecture. *Sensors*, *22*(12), 4649. doi:10.3390/s22124649.